The International Journal of **Medical Robotics** and **Computer Assisted Surgery**

THE INTERNATIONAL JOURNAL OF MEDICAL ROBOTICS AND COMPUTER ASSISTED SURGERY
Int J Med Robotics Comput Assist Surg (2011)
Published online in Wiley Online Library (wileyonlinelibrary.com) **DOI:** 10.1002/rcs.442

ORIGINAL ARTICLE

Synchronization of epicardial crawling robot with heartbeat and respiration for improved safety and efficiency of locomotion

Nicholas A. Patronik[1]
Takeyoshi Ota[2]
Marco A. Zenati[2]
Cameron N. Riviere[1]*

[1]*The Robotics Institute, Carnegie Mellon University, Pittsburgh, PA, USA*

[2]*Department of Surgery, University of Pittsburgh, Pittsburgh, PA, USA*

*Correspondence to: Cameron N. Riviere, The Robotics Institute, Carnegie Mellon University, Pittsburgh, PA 15213 USA.
E-mail: camr@ri.cmu.edu

Accepted: 12 September 2011

Abstract

Background HeartLander is a miniature mobile robot designed to navigate over the epicardium of the beating heart for minimally invasive therapy. This paper presents a technique to decrease slippage and improve locomotion efficiency by synchronizing the locomotion with the intrapericardial pressure variations of the respiration and heartbeat cycles.

Methods Respiratory and heartbeat phases were detected in real time using a chest-mounted accelerometer during locomotion in a porcine model *in vivo*. Trials were conducted over the lateral aspect of the heart surface to test synchronized locomotion against an unsynchronized control.

Results Offline evaluation showed that the respiration and heartbeat algorithms had accuracies of 100% and 88%, respectively. Synchronized trials exhibited significantly lower friction, higher efficiency, and greater total distance traveled than control trials.

Conclusion Synchronization of the locomotion of HeartLander with respiration and heartbeat is feasible and results in safer and more efficient travel on the beating heart. Copyright © 2011 John Wiley & Sons, Ltd.

Keywords robot; minimally invasive; beating heart; epicardial therapy

Introduction

Minimally invasive beating-heart therapy requires precise and stable manipulation on an organ with complex, rapid motion in a confined environment (1,2). This technique can be augmented with teleoperated instrumentation, through which the motions of the surgeon's hands are mimicked by a set of robotically actuated tools located inside the patient (3,4). Although these robotic systems improve upon conventional thoracoscopy by increasing dexterity, restoring hand–eye coordination, and reducing fatigue, they have difficulties caused by organ motion and access limitations when used in beating-heart surgery (5).

Several researchers are attempting to compensate organ motion in robot-assisted coronary artery bypass grafting surgery through active compensation of heartbeat motion by tracking the epicardium and moving the tool tips accordingly (6–9). This remains an open research problem; challenges include modeling or tracking the heart surface, and high-bandwidth actuation in at least three degrees of freedom (DOFs) over a relatively large workspace.

To address the need for organ motion compensation and improved access, and to further reduce patient morbidity, we have developed a miniature mobile

robot, called HeartLander, that can adhere to and travel over the heart surface for the delivery of therapy from a single incision (10). We envision that HeartLander could be useful for therapies that require flexible tools and can be completed from within the pericardial sac; examples include the injection of regenerative materials for heart failure (11), lead placement for resynchronization (12), and epicardial ablation for arrhythmia (13). As proofs of concept, HeartLander has successfully deployed injection needles (10), pacing leads (14), and ablation catheters (15) on the beating heart with the chest closed in a porcine model *in vivo*.

HeartLander has demonstrated precise target acquisition at specified locations on the anterior, lateral, and posterior surfaces of a closed-chest beating-heart porcine model through a single percutaneous subxiphoid incision (16). Although locomotion to the target areas was successful, the efficiency was only 40%, due to slippage on the heart surface (16). Slippage is clearly an impediment to effective navigation, but also represents a safety concern due to repeated abrasion of the epicardium. Experiments with ovine hearts *in vitro* have suggested that the epicardial membrane is not damaged if HeartLander slides over it a small number of times, but that repeated passage over the same location while suction is active can eventually cause damage (15). This paper presents an investigation of the feasibility of improving efficiency, and thereby also safety, by synchronizing the locomotion mechanics with the physiological motion of the heart.

Locomotion of HeartLander

HeartLander is an inchworm-like robot crawler that uses suction to grip the epicardial surface of the heart, and drive-wire actuation of tandem body sections to generate motion (Figure 1). The tethered design of the crawler allows for the transmission of relatively high suction and drive wire forces from offboard instrumentation. Each body section is $5.5 \times 8 \times 8$ mm (H × W × L), giving the crawler a length of 16 mm when fully contracted. The vacuum pressure used to grip the heart ranges from 400 to 550 mmHg, which has been proven to be safe and effective in FDA-approved cardiac stabilizers (17,18). The two nitinol drive wires are 0.3 mm in diameter, and are linearly actuated by two offboard stepper motors (M23, US Digital Corp.) to change the distance between the two crawler body sections. One cycle of the locomotion scheme is as follows: (a) release grip on the front body; (b) advance the front body by extending the drive wires; (c) switch the suction grip from the rear body to the front body; and (d) advance the rear body by retracting the drive wires. This scheme is illustrated in Figure 2. The rear body advances when the wires are retracted because the wires are encapsulated by flexible plastic sheaths between the rear body and the offboard motor stage. Thus the wire translations at the motor stage are transmitted to wire translations between the bodies. The two drive wires provide two degrees of freedom to navigate over the surface of the heart. The pericardial sac enclosing the heart provides the normal force required for the robot to remain in contact with the heart surface during operation, thus reducing navigation to a 2D task.

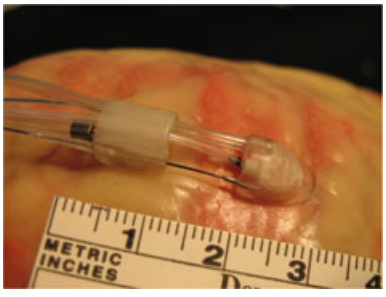

Figure 1. Photograph of the HeartLander crawler robot on a rubber beating heart model

Physiological motion

Although the heart moves within the pericardium during beating, it is surrounded by structures on all sides. In the coronal body plane, the heart is enclosed by the lungs, the diaphragm, and the great vessels. In the axial plane, it is bounded by the lungs, esophagus, spinal column, and sternum. Accordingly, there is no free space around the heart *in situ*. Furthermore, the pericardium tightly encloses the heart, with only a 0.5 mm layer of pericardial fluid separating the two (19). The pericardium has a nonlinear stress–strain characteristic that causes it to expand readily during the initial filling phase of the heartbeat cycle, then stiffen greatly to provide restraint as the heart fills with blood and enlarges (20).

The surface pressure generated by the pericardium on the heart fluctuates over the cardiac and respiratory cycles. The cardiac cycle is made up of two primary phases: *diastole*, during which the heart fills with blood, and *systole*, when the blood is ejected from the heart. Measurements of intrapericardial pressure in humans have shown a range of 0–17 mmHg over the cardiac cycle (21). This pressure variation is due to the fact that the total heart volume varies 8–10% over the cardiac cycle (22,23). The heart volume reaches a minimum at the end of systole, as does also the intrapericardial pressure.

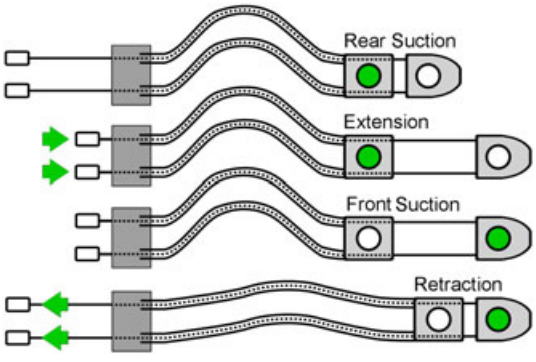

Figure 2. Illustration of one cycle of the HeartLander locomotion scheme. Dark circles indicate active suction grip

DOI: 10.1002/rcs

Intrapericardial pressure also fluctuates over the respiratory cycle by 2–6 mmHg (24,25). The respiratory cycle is composed of *inspiration*, when the lungs fill with air, and *expiration*, when air is expelled. The underlying physiological cause of this pressure fluctuation may be the displacement of the heart in the anteroposterior direction, which varies the degree to which the pericardium is stretched over the heart. Additionally, the lung volume varies over the respiratory cycle, and thus may exert a varying external pressure on the pericardium and heart. These factors cause the minimal intrapericardial pressure over the respiratory cycle to occur at the end of expiration.

These variations in pericardial pressure that are driven by the cardiac and respiratory cycles result in variation of the normal force exerted on the heart surface and thus on HeartLander. This variable normal force imparted by the pericardium on HeartLander generates a friction force between the crawler and surrounding intrapericardial tissue, which resists extension and retraction of the bodies during locomotion.

Locomotion efficiency

Traction loss or slippage occurs when the force required to extend or retract the drive wires exceeds the traction force provided by the suction gripper of the body section that has active suction at the time. If the rear body slips backwards during wire extension, the front body will not advance by the full length of the wire displacement. Likewise, if the front body slips backwards during wire retraction, the rear body will not advance by the full length of wire displacement. Slippage reduces the efficiency of locomotion, can make certain regions of the heart difficult to access at all, and can cause damage to the heart surface through repeated abrasion (15). To avoid slipping, the traction force must overcome the friction force imparted on the moving body section by the pericardium and epicardial surface of the heart.

The vacuum pressure that generates the surface traction must remain within the range established to be safe for the epicardial surface (17), and thus cannot be arbitrarily increased to improve traction. An alternative method to improve locomotion efficiency is to reduce the normal force of the pericardium on HeartLander, thus reducing the friction force experienced during motion. In this paper we describe our effort to improve efficiency by synchronizing the locomotion cycle with the natural variations in intrapericardial pressure, such that the robot moves when the normal force, and thus friction force, is at its minimum.

Materials and Methods

Locomotion synchronization

To minimize the friction force exerted on HeartLander by the pericardium, the robot must initiate and complete each step motion within the end-expiration and end-systole phases of the respiratory and cardiac cycles. Accordingly, these phases must be accurately detected in real time. When it has been determined that both of the physiological cycles are within the specified phase ranges, the step synchronization algorithm will allow an extension or retraction event to commence if requested by the locomotion control system. The general architecture of this step synchronization algorithm is presented in Figure 3.

Accelerometer placement

The data from a triaxial accelerometer (CXL02LF3, Crossbow Technology Inc.) were used to detect the heartbeat and respiration phases in the synchronization algorithms. Accelerometer data were sampled at 100 Hz.The optimal placement of the accelerometer on the porcine model was determined experimentally under a board-approved protocol. The accelerometer was affixed to seven locations on the surface of the porcine chest, and data sets were recorded for one minute at each location (Figure 4(a)). The amplitude spectra of the three accelerometer axes were examined at each of the seven locations. The highest peaks at the known frequencies of respiration (0.267 Hz) and heartbeat (1.55 Hz) were both found at the superior left sternum (location #7 in Figure 4(a)). The highest peak at the heartbeat frequency was found in the z-axis data (normal to the skin surface) at this location (Figure 4(c)). The highest peak at the respiration frequency was found in the x-axis data (Figure 4(b)), tangential to the chest surface. These results differed from the optimal accelerometer placement reported for the human anatomy (26).

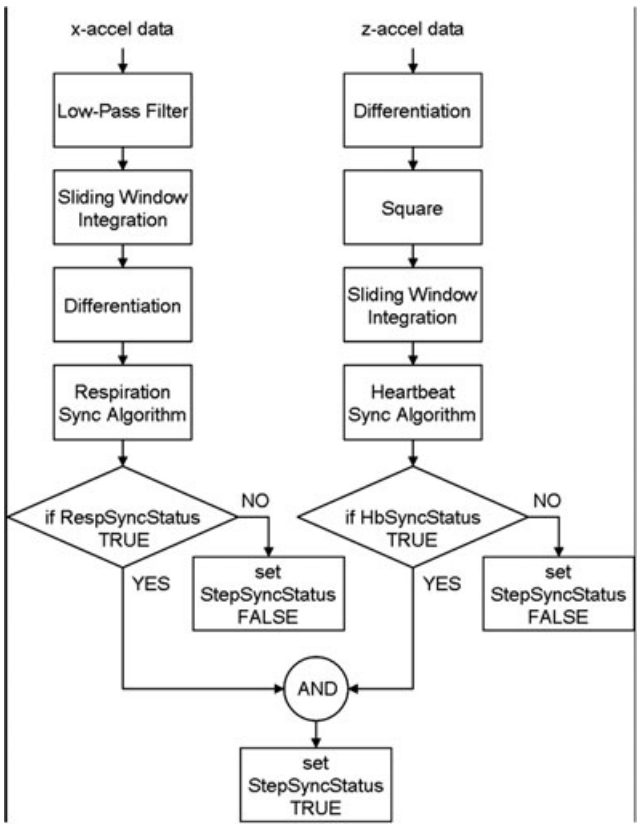

Figure 3. The step synchronization algorithm

DOI: 10.1002/rcs

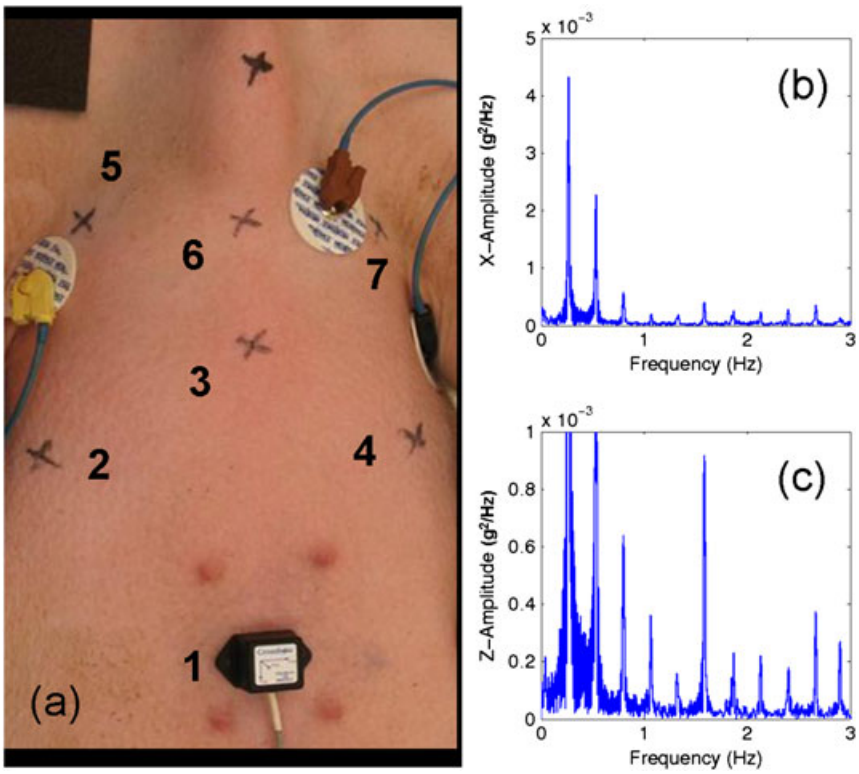

Figure 4. (a) The seven accelerometer locations evaluated for optimal signal strength on the porcine chest. (b) The amplitude spectrum of the *x*-axis accelerometer data at location #7, with the largest respiration frequency peak. (c) The amplitude spectrum of the *z*-axis accelerometer data at location #7, with the largest cardiac frequency peak

Given the small translational acceleration due to respiration, it is evident from the relative magnitudes of the peaks in Figure 4 that the accelerometer responded to the changing gravitational component of acceleration as the chest wall moved; i.e. in the case of respiration it served largely as a tilt sensor.

Respiration synchronization

The respiration synchronization algorithm determined the respiratory cycle phase from the accelerometer data, and passed that information to the step synchronization algorithm. A diagram of the respiration synchronization algorithm is given in Figure 5(a).During testing, the animal was ventilated at a rate of 12–16 breaths per minute. The ventilation settings were such that inspiration comprised the first third of the cycle, expiration the second third, and a pause the final third. This resulted in one third of the respiratory cycle spent in end-expiration, during which time the respiratory component of intrapericardial pressure was minimal. Over the range 12–16 breaths per minute, this corresponded to a range of 1.25–1.67 seconds during which stepping could be optimally coordinated with the respiratory cycle. We adopted the respiratory phase value notation of Shechter *et al.* (27), such that the inspiration phase had a value range 0 to 1 and the expiration phase a range −1 to 0. For the purpose of synchronizing the locomotion, we set the final 75% of the expiration phase as acceptable, including the second half of the expiratory motion and the ensuing pause. This corresponded to a respiratory synchronization phase range −0.75 to 0. The phase values over the entire respiratory signal were determined by detecting the phase at one particular point in the cycle (i.e. end-expiration), then interpolating based on the known output of the ventilator. This detection method requires one full respiration cycle to initialize.

To prepare the accelerometer data for respiratory phase detection, the x-axis signal of the accelerometer was first filtered with a third-order Chebyshev type II low-pass filter with a 5 Hz cutoff frequency and 20 dB stopband ripple. This filter removed high frequency noise while introducing a delay of less than 50 ms. A moving-window integration or summing filter with a window length of 0.8 s (the average length of one heartbeat period) was then applied in order to smooth out the heartbeat component. Lastly, the filtered data were differentiated. (Since the accelerometer acted largely as a tilt sensor in the case of respiration, this differentiated signal largely represented an angular rate signal.)

This differentiated signal was then input to the respiration synchronization algorithm (Figure 5(a)). The algorithm detected the end of the expiratory motion by locating the zero crossing in the negative direction. When this event was detected, the respiration sync status was set to TRUE. The algorithm then began incrementing a counter for each iteration of the control cycle. When this counter exceeded the duration of the expiration phase, the respiration sync status variable was set back to FALSE. The respiration sync status value was recorded, along with all other data, for offline evaluation of the algorithm accuracy.

Heartbeat synchronization

The heartbeat synchronization algorithm coordinated the stepping motions around the end of the systolic phase, at

DOI: 10.1002/rcs

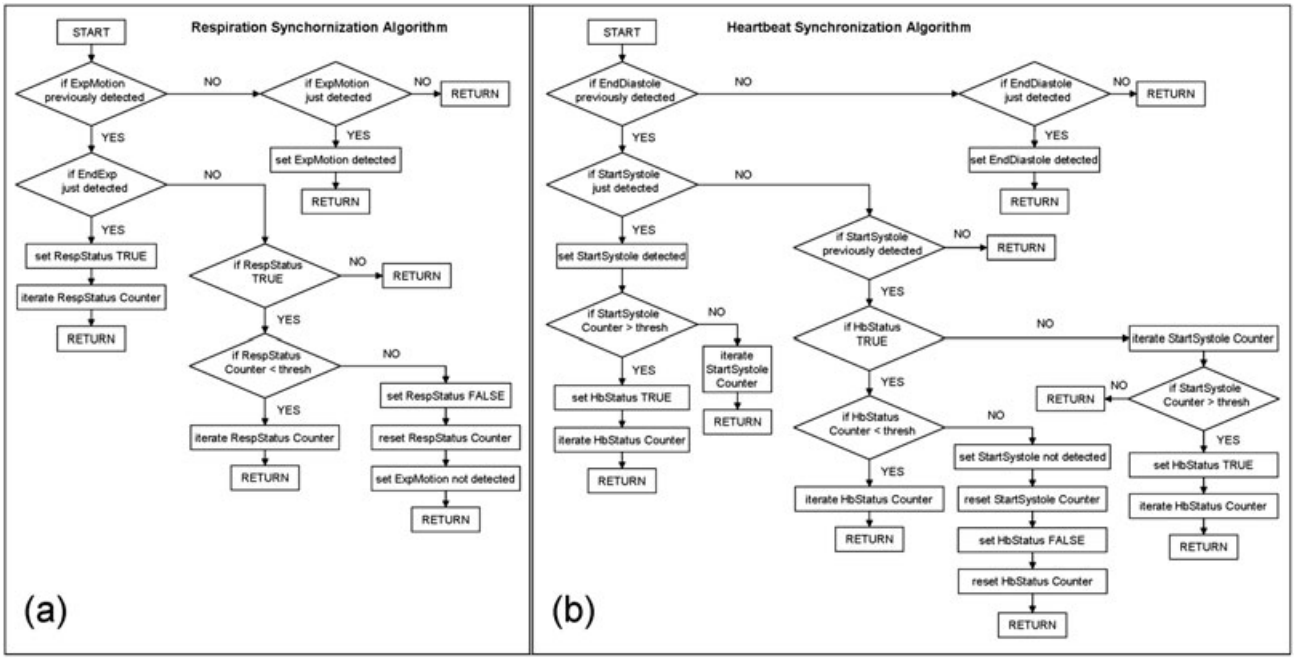

Figure 5. (a) Architecture of the respiration synchronization algorithm. (b) Architecture of the heartbeat synchronization algorithm

which point the heart volume was minimal (Figure 5(b)). The heart rate range for our porcine model was 60–120 beats per minute (1.0–2.0 Hz), which corresponded to a heartbeat period range of 0.5–1.0 s. We adopted the cardiac phase value convention of Shechter *et al.*, with a systolic phase range 0–0.42 and a diastolic range 0.42–1.0 (27). Allowing one-half of the full cardiac cycle for stepping, centered around end systole, led to an acceptable cardiac phase value range 0.17–0.67 for the heartbeat synchronization algorithm.

The z-axis accelerometer data were processed and input to the heartbeat synchronization algorithm for the detection of systole (Figure 3). Prior to being input to the algorithm, the accelerometer data were processed in a similar manner to ECG data for the well-known Pan Tompkins real-time QRS detector (28). The data were first differentiated to provide the slope of the accelerometer data. These data were then squared, making all data positive and amplifying the acceleration slope in a nonlinear fashion to emphasize the higher frequencies – such as the heart contraction motion of systole. Lastly, a moving window integration filter was applied. The filter width was set to 30 samples, which corresponded to the maximum width of the systolic motion waveform based on the animal heart rate measured at the onset of testing.

The processed z-axis accelerometer data were then fed into the heartbeat synchronization algorithm (Figure 5(b)). The start of the systolic motion was detected when the value exceeded an experimentally determined threshold ($0.0012\,m^2/s^5$), which indicated the high-speed ventricular contraction motion. The synchronization algorithm then began iterating a counter, which was used to locate the previously specified phase range 0.17–0.67 and set the heartbeat sync status to TRUE. A second counter was used to time the end of the desired heartbeat phase range, based on the heart rate of the specific porcine model as indicated by the ECG. The synchronization status data were recorded for offline evaluation of the accuracy of the algorithm.

Porcine model evaluation

A healthy swine (45 kg) was used in an animal study, in accordance with a board-approved protocol, to evaluate the accuracy of the synchronization algorithms and the resulting locomotion performance. The heart was allowed to beat naturally, without the use of anti-arrhythmic drugs. The animal was placed on a ventilator, and breathing was regulated at 0.2 Hz. The surgeon accessed the apex of the heart through an incision beneath the sternum, and placed HeartLander on the epicardium through a second small incision in the pericardium. This subxiphoid approach provided intrapericardial access for the robot on the beating heart without requiring differential ventilation or lung deflation. Additional clinical details can be found in (10).

The synchronization accuracy was evaluated on the beating porcine model through a series of locomotion trials. All trials were conducted over the same portion of the lateral wall of the left ventricle. Each locomotion trial consisted of five steps from the apex toward the base of the heart. The commanded length of each step was 15 mm, and the commanded step speed was 25 mm/s. Synchronization was active for 10 locomotion trials and inactive for 10 control trials. Synchronized and control trials were alternated.

Synchronization evaluation

The respiration and heartbeat synchronization algorithms were evaluated by calculating the percentage of synchronized step events that fell within the specified acceptable phase ranges during testing on our animal model. To

DOI: 10.1002/rcs

provide an independent measure of the true physiological phase values at the step events, offline detection methods were established for all respiratory and cardiac events during testing. Noncausal zero-phase filtering methods (Matlab `filtfilt`) were used to assist the online detection. For respiration, the end-expiration events were detected offline using the filtered electromagnetic tracking data. The respiration phases were clear in the tracking data due to the regularity and the relatively low frequency of the respiration cycle. ECG was used as the offline gold standard for the detection of end-systole in the cardiac cycle. The Pan-Tompkins detector was used to locate the QRS complex of each heartbeat, which corresponds with the start of systole (28).

The offline respiratory and cardiac phase values were calculated for all steps from all locomotion trials. Specifically, the phases were calculated for the initiation and completion of each step extension and retraction. These phase values were then evaluated to determine whether or not they fell within the specified acceptable respiratory and cardiac phase ranges. The percentage of step events that was properly synchronized with the respiration cycle and heartbeat cycle was independently calculated. In this manner, the accuracy of the respiratory and cardiac synchronization algorithms was evaluated. The percentage of properly synchronized step events was also calculated for the control trials, during which synchronization was inactive.

Locomotion evaluation

The locomotion efficiency was also evaluated during the locomotion trials on the porcine model. The front body of the robot contained a 6-DOF electromagnetic tracking sensor (microBIRD, Ascension Technology Corp.) that was used to provide real-time visualization of the robot location on a computer model of the heart surface during the trials. The reported accuracy of the tracking system is 1.4 mm. We opted not to use this sensor for the physiological cycle phase detection, since the accelerometer offered higher bandwidth (29). The data from the tracking sensor were also used offline to calculate the step extension efficiency, step retraction efficiency, total step efficiency, and distance traveled. The underlying physiological artifacts in the robot tracker motion were attenuated with a sliding-average filter.

Each step of the crawler comprised an extension and retraction event, both of which had the same command step length. During extension, the front body ideally advanced from its initial location by the commanded step length, while the rear body remained fixed at its initial position. During retraction, the rear body of the crawler ideally advanced by the commanded step length, while the front body remained fixed at its location following extension. Thus each step advanced the crawler by one full commanded step length if the total efficiency of the step was 100%. Since only the front body contained a tracker, due to size constraints, all efficiencies (extension, retraction, and total) were calculated from the motion of the front body. The efficiency during the extension portion of a step was calculated as

$$\eta_{ext} = \frac{d_{ext}}{l} \tag{1}$$

where d_{ext} is the measured displacement of the front body section, normalized by the commanded step length l. The efficiency during the retraction portion of a step was calculated as one minus the measured displacement of the front body section – which should not have moved during retraction – normalized by the commanded step length

$$\eta_{ret} = 1 - \frac{d_{ret}}{l} \tag{2}$$

The total step efficiency was calculated as the difference between the extension and retraction motions, normalized by the commanded step length

$$\eta_{total} = \frac{d_{ext} - d_{ret}}{l} \tag{3}$$

The distance traveled was calculated as the resultant motion in the forward and vertical directions, relative to the robot. The lateral component of the robot motion was not included in the calculation of distance traveled, as it did not contribute to the progress of the robot over the heart surface. The peak extension and retraction forces were also calculated from load cells that were integrated into the actuation mechanism.

The values for each of these six parameters were averaged at each step and over the entire path for both the control and synchronized trial sets ($n = 10$). The average values of these parameters for the control and synchronized trial sets were then compared at each step and over the entire path using the Mann–Whitney–Wilcoxon test. This non-parametric test assesses the probability that two sets of observations come from the same distribution, without assuming a normal sample distribution. We considered a p-value less than 0.05 to be sufficient to establish significance of the difference between the control and synchronized results.

Results

The animal survived until the end of the procedure, at which point it was euthanized according to the board-approved protocol. No adverse hemodynamic or electrophysiological events were observed. Only superficial suction marks were noted on the epicardium, which have been shown to be temporary (10).

The respiration and heartbeat synchronization accuracy of all stepping events from the synchronization and control trials were calculated using the offline phase detections as the reference. Figures 6 and 7 demonstrate the offline respiration and cardiac phase values calculated for each of the extension and retraction step events in two, single locomotion trials. The previously defined acceptable phase ranges for the respiratory cycle (−0.75 to 0) and cardiac cycle (0.17 to 0.67) are shown by the green bands on each plot.

DOI: 10.1002/rcs

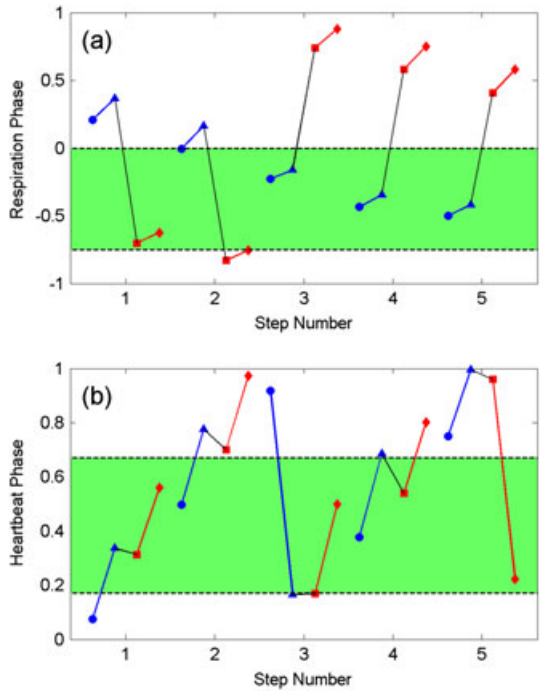

Figure 6. (a) The respiration phase values for all step events of a single unsynchronized control locomotion trial. Extension starts are shown by blue circles, extension ends by blue triangles, retraction starts by red squares, and retraction ends by red diamonds. The respiration phase ranges from end-inspiration (−1,+1) to end-expiration (0). (b) The heartbeat phase values for the extension and retraction events of a single unsynchronized control trial. The heartbeat phase ranges from end-diastole (0,+1) to end-systole (0.42). The acceptable phase ranges for both respiration and heartbeat are shown by the green highlighted region between the horizontal broken lines

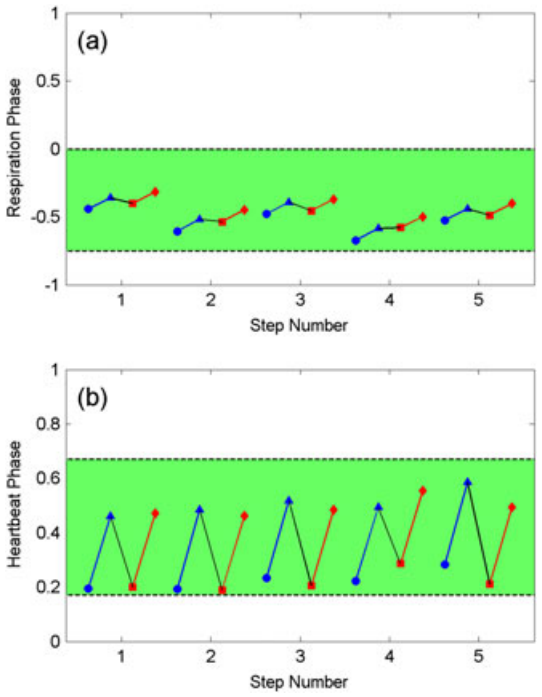

Figure 7. (a) The respiration phase values for all step events of a single synchronized locomotion trial. Extension starts are shown by blue circles, extension ends by blue triangles, retraction starts by red squares, and retraction ends by red diamonds. The respiration phase ranges from end-inspiration (−1,+1) to end-expiration (0). (b) The heartbeat phase values for the extension and retraction events of a single synchronized trial. The heartbeat phase ranges from end-diastole (0,+1) to end-systole (0.42). The acceptable phase ranges for both respiration and heartbeat are shown by the green highlighted region between the horizontal broken lines

The connected blue circle–triangle pairs show the initiation and completion of each extension, while the connected red square–diamond pairs show the retraction endpoints. Each extension–retraction pair, connected by a black line, comprises a complete step event. In Figure 6, the lack of step event synchronization with the physiological phases for the control trial is evident. In contrast, the step events for the synchronized trial shown in Figure 7 all lie within the specified physiological phase bounds.

Figures 8 and 9 are histograms of the offline respiration and cardiac phase values for the step events from all the control and synchronized trials, with the acceptable physiological phase boundaries shown by broken vertical lines. From Figure 8, it is clear that the step events were distributed approximately evenly over the entire respiration and heartbeat phase ranges. Conversely, Figure 9 shows that the step events from the synchronized locomotion trials were entirely within the acceptable phase range for respiration, and largely within the acceptable range for heartbeat. The step events that fell outside the specified cardiac phase range signify errors in the heartbeat synchronization algorithm. The accuracies of the respiration, heartbeat, and total step synchronization algorithms that were calculated for all step events over the synchronized and control trial sets can be found in Table 1.

The values of the locomotion efficiency parameters can be found in Table 2. Figure 10 shows the values of the parameters averaged at each step for the control and synchronized trial sets, with standard deviations shown by error bars. The *p*-values for these comparisons at each step and over the total path can also be found in Table 2. The locomotion efficiency parameters explored in this analysis all showed statistically significant improvements with physiological synchronization, with the exception of step extension efficiency.

Discussion

A minimally-invasive crawling robot with navigation capabilities may prove to be a clinically useful delivery vehicle for therapy on the epicardial surface of the beating heart. In order to serve in this capacity, HeartLander must be able to safely navigate to remote locations on the heart surface from its insertion near the apex while carrying a clinical payload. Improving the locomotion efficiency addresses this goal by maximizing the distance the crawler can travel, and thus the set of locations the crawler can feasibly reach, and by increasing the clinical payload capacity. Furthermore, improved efficiency reduces unnecessary repeated abrasion that may damage

DOI: 10.1002/rcs

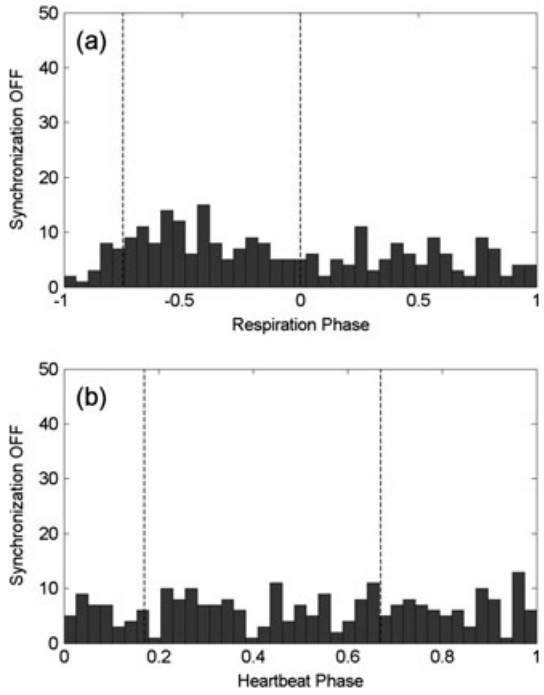

Figure 8. (a) The respiration phase values and (b) heartbeat phase values for the extension and retraction events of all unsynchronized control trials. The respiration phase ranges from end-inspiration (−1,+1) to end-expiration (0). The heartbeat phase ranges from end-diastole (0,+1) to end-systole (0.42). The acceptable phase ranges for both respiration and heartbeat are between the vertical broken lines

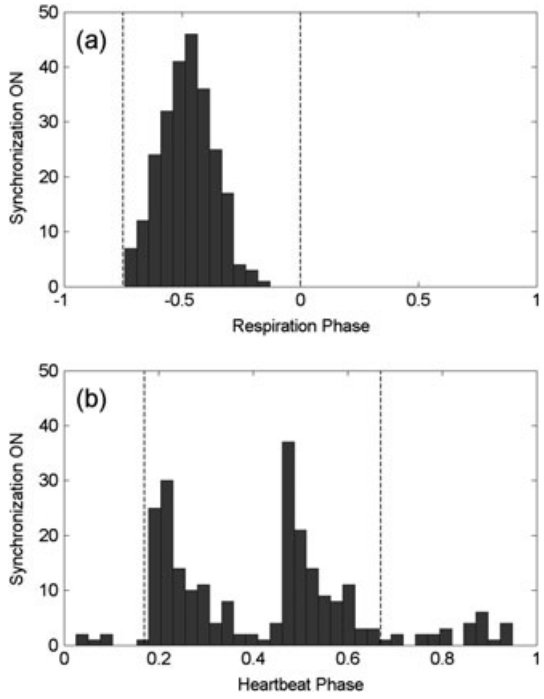

Figure 9. (a) The respiration phase values and (b) heartbeat phase values for the extension and retraction events of all synchronized trials. The respiration phase ranges from end-inspiration (−1,+1) to end-expiration (0). The heartbeat phase ranges from end-diastole (0,+1) to end-systole (0.42). The acceptable phase ranges for both respiration and heartbeat are between the vertical broken lines

the epicardium over time. Because the period of time required for one complete locomotion cycle is comparable with the period of the cardiac cycle, it has been observed that when operating without synchronization, if the crawler happens to initiate a step at the least favorable phase in the cardiac cycle, it can sometimes remain so for many cycles, maximizing slippage; clearly, synchronization avoids this problem.

The respiration and heartbeat synchronization algorithms were generally successful in synchronizing locomotion with the desired respiratory and cardiac phase ranges. The data from the skin-mounted triaxial accelerometer were sufficient to measure and identify the mechanical events associated with the various phases of both respiration and heartbeat. Of the 200 step events (initiation and completion of every extension and retraction) from the ten synchronized trials, 100% were correctly synchronized with respiration and 88% with heartbeat, versus 52% and 50%, respectively, from the control trials. Given that half of each phase range was deemed acceptable, it is reasonable that approximately half of the step events from the unsynchronized trial set falls within these phase ranges. The complete synchronization algorithm correctly synchronized 88% of the step events with both respiration and heartbeat, compared with only 26% of the step events from the control trials. An accuracy of one-quarter was expected for the unsynchronized trials, as that is the fraction of the total physiological cycle covered by the overlapping acceptable ranges. The step events incorrectly synchronized with heartbeat included a number of steps that were initiated at the correct phase value, but failed to complete within the acceptable phase range due to an irregularly timed contraction of the subsequent heartbeat. In the future, detection of such events can be performed and used to trigger immediate termination of the step motion in progress.

The step event synchronization caused statistically significant improvements in all but one of the locomotion parameters evaluated. Our hypothesis was that locomotion efficiency would improve by synchronizing the locomotion extensions and retractions with the physiological motion phase range corresponding to minimum pericardial pressure and thus minimum friction force on HeartLander. The retraction efficiency increased by 14% for the synchronized trial set over the control set, while the total step efficiency increased by 27%. Both efficiency increases were found to be statistically significant. Unsurprisingly, the total distance traveled was 31% greater for the synchronized trial set, which was a statistically significant improvement. The statistically significant decreases in extension and retraction peak forces validated the hypothesis that synchronization with the end-expiration and end-systole phases would result in decreased friction forces experienced by the crawler. These decreases in force (13% for extension and 27% for retraction) provide a physical explanation for the corresponding efficiency increases during both phases of locomotion. We believe that the extension efficiency did not significantly improve with the decrease in friction on the front body because the friction of the tether helped

DOI: 10.1002/rcs

Table 1. Percentage of step events that were properly synchronized with respiration and heartbeat from the control and synchronized trial sets

	Extension Start (%)	Extension Stop (%)	Retraction Start (%)	Retraction Stop (%)	Average (%)
Sync OFF – Respiration Accuracy	66	73	36	32	52
Sync OFF – Cardiac Accuracy	55	45	52	48	50
Sync OFF – Combined Accuracy	36	34	18	18	26
Sync ON – Respiration Accuracy	100	100	100	100	100
Sync ON – Cardiac Accuracy	94	84	98	74	88
Sync ON – Combined Accuracy	94	84	98	74	88

Table 2. Vlues of the locomotion parameters averaged over each step and over the entire path for the control and synchronized trial sets (asterisks indicate statistically significant results)

	Averaged over Total Path	*p*-value
Extension Efficiency – Sync OFF (%)	68	0.22
Extension Efficiency – Sync ON (%)	73	
Retraction Efficiency – Sync OFF (%)	66	0.01*
Retraction Efficiency – Sync ON (%)	75	
Total Efficiency – Sync OFF (%)	39	0.049*
Total Efficiency – Sync ON (%)	50	
Distance Traveled – Sync OFF (mm)	37	0.01*
Distance Traveled – Sync ON (mm)	45	
Peak Extension Force – Sync OFF (N)	4.6	0.003*
Peak Extension Force – Sync ON (N)	4.0	
Peak Retraction Force – Sync OFF (N)	4.6	0.000*
Peak Retraction Force – Sync ON (N)	3.4	

anchor the rear body, improving traction and minimizing the amount of additional improvement that the synchronization could provide. During retraction, on the other hand, this same tether friction must be overcome in order to advance the rear body. Thus, the decrease in friction force on the rear body and tether that resulted from synchronization caused an increase in the retraction efficiency from 66% to 75%.

In the current study, the step speed, commanded step length, and timing were set based on the heart rate measured at the start of testing. However, heart rate is known to vary over time. Dynamic tracking of the heart rate could be used to modulate these parameters accordingly, and would likely also make cardiac event detection more accurate and robust. Physiological sensors such as ECG leads and air flow sensors, which are readily available in a surgical suite, can be used to augment the accelerometer data (30). If needed, to further improve locomotion efficiency, the acceptable phase regions for respiration and heartbeat can be narrowed, granting, however, that this requires more accurate event detection. In the long term, respiration and heartbeat synchronization algorithms must also be established or adapted for the human body (7). This study was performed while the subject was in normal sinus rhythm; arrhythmia represents a different challenge, of course, which must also be addressed in the longer term.

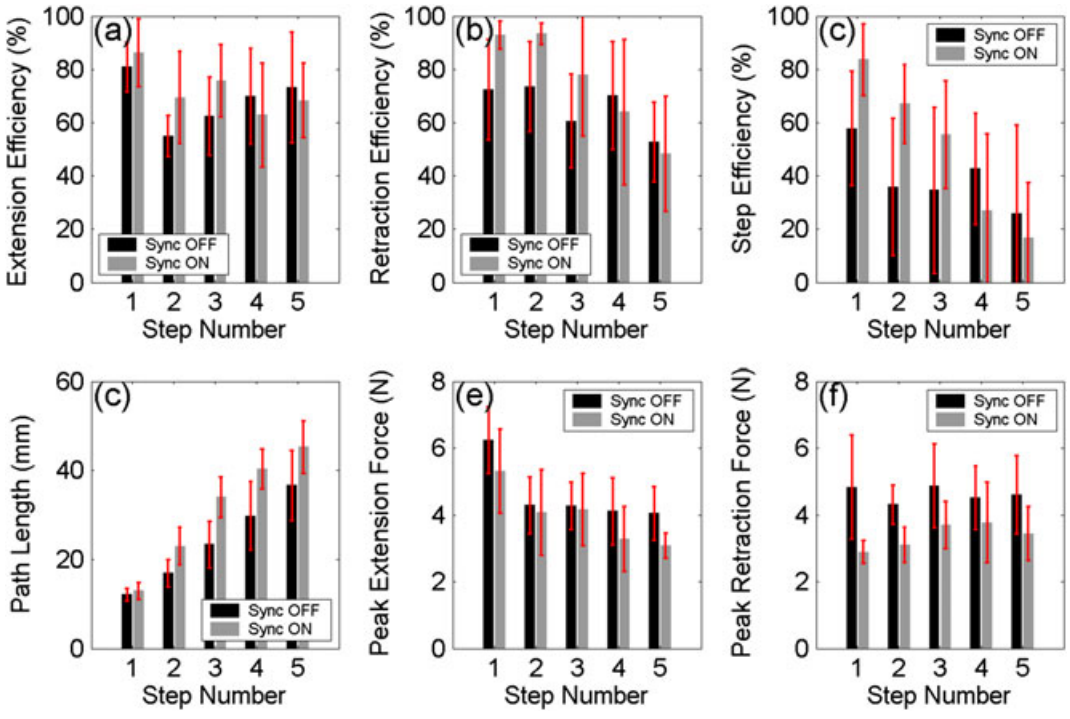

Figure 10. The locomotion parameters averaged over each step for the control and synchronized trial sets. The values of (a) extension efficiency, (b) retraction efficiency, (c) step efficiency, (d) distance traveled, (e) peak extension force, and (f) peak retraction force

DOI: 10.1002/rcs

Conclusion

By synchronizing the locomotion of a robotic crawler with the heartbeat and respiration, the friction forces imparted on the robot by the surrounding physiological environment were significantly decreased. The decrease in friction led to significant improvements in locomotion efficiency and thereby in total distance traveled. This has the effect of increasing the total region on the epicardial surface that can be safely reached by the robot.

Acknowledgements

This work was supported in part by the National Institutes of Health (grant no. R01 HL078839) and the National Aeronautics and Space Administration (grant no. NNG05GL63H).

Conflict of interest

N. A. P., M. A. Z., and C. N. R. are co-inventors of HeartLander and hold equity in HeartLander Surgical, Inc. (licensee of the IP from Carnegie Mellon University).

References

1. Cattin P, Dave H, Grunenfelder J, *et al*. Trajectory of coronary motion and its significance in robotic motion cancellation. *Eur J Cardiothorac Surg* 2004; **25**: 786–790.
2. Lemma M, Mangini A, Redaelli A, Acocella F. Do cardiac stabilizers really stabilize? Experimental quantitative analysis of mechanical stabilization. *Interact Cardiovasc Thorac Surg* 2004; **4**: 222–226.
3. Caynak B, Sagbas E, Onan B, *et al*. Robotically enhanced coronary artery bypass grafting: the feasibility and clinical outcome of 196 procedures. *Int J Med Robotics Comput Assist Surg* 2009; **5**: 170–177.
4. Casula R, Athanasiou T, Darzi A. Minimal access coronary revascularization without cardiopulmonary bypass-the impact of robotic technology in the current clinical practice. *Int J Med Robotics Comput Assist Surg* 2004; **1**(1): 98–106.
5. Damiano RJ, Jr. Robotics in cardiac surgery: the emperor's new clothes. *J Thorac Cardiovasc Surg* 2007; **134**(3): 559–561.
6. Bachta W, Renaud P, Cuvillon L, *et al*. Motion prediction for computer-assisted beating heart surgery. *IEEE Trans Biomed Eng* 2009; **56**(11): 2551–2563.
7. Bebek O, Cavusoglu MC. Intelligent control algorithms for robotic-assisted beating heart surgery. *IEEE Trans Robot* 2007; **23**(3): 468–480.
8. Gangloff J, Ginhoux R, de Mathelin M, *et al*. Model predictive control for compensation of cyclic organ motions in teleoperated laparoscopic surgery. *IEEE Trans Control Systems Technol* 2006; **14**(2): 235–246.
9. Ortmaier T, Groeger M, Boehm DH, *et al*. Motion estimation in beating heart surgery. *IEEE Trans Biomed Eng* 2005; **52**(10): 1729–1740.
10. Ota T, Patronik NA, Schwartzman D, *et al*. Minimally invasive epicardial injection using a novel semiautonomous robotic device. *Circulation* 2008; **118**: S115–S120.
11. Kocher AA, Schuster MD, Szabolcs MJ, *et al*. Neovascularization of ischemic myocardium by human bone-marrow-derived angioblasts prevents cardiomyocyte apoptosis, reduces remodeling and improves cardiac function. *Nat Med* 2001; **7**(4): 430–436.
12. Dekker LAJ, Phelps B, Dijkman B, *et al*. Epicardial left ventricular lead placement for cardiac resynchronization therapy: optimal pace site selection with pressure-volume loops. *J Thorac Cardiovasc Surg* 2004; **127**: 1641–1647.
13. Sosa E, Scanavacca M. Epicardial mapping and ablation techniques to control ventricular tachycardia. *J Cardiovasc Electrophysiol* 2005; **16**: 449–452.
14. Ota T, Patronik N, Schwartzman D, *et al*. Subxiphoid epicardial pacing lead implantation using a miniature crawling robotic device. *J Surg Res* 2007; **137**(2): 242–243.
15. Patronik NA. A miniature mobile robot for precise and stable access to the beating heart. PhD dissertation, Carnegie Mellon University, Pitsburg. Robotics Institute Tech. Report no. CMU-RI-TR-08-13, 2008.
16. Patronik NA, Ota T, Zenati MA, Riviere CN. A miniature mobile robot for navigation and positioning on the beating heart. *IEEE Trans Robotics* 2009; **25**(5): 1109–1124.
17. Borst C, Jansen EW, Tulleken CA, *et al*. Coronary artery bypass grafting without cardiopulmonary bypass and without interruption of native coronary flow using a novel anastomosis site restraining device ("Octopus"). *J Am Coll Cardiol* 1996; **27**: 1356–1364.
18. Jansen EWL, Lahpor JR, Borst C, *et al*. Off-pump coronary bypass grafting: how to use the Octopus Tissue Stabilizer. *Ann Thorac Surg* 1998; **66**(2): 576–579.
19. Santamore WP, Constantinescu MS, Bogen D, Johnston WE. Nonuniform distribution of normal pericardial fluid. *Basic Res Cardiol* 1990; **85**(6): 541–549.
20. Vito RP. The role of the pericardium in cardiac mechanics. *J Biomech* 1979; **12**: 587–592.
21. Tyberg JV, Taichman GC, Smith ER, *et al*. The relationship between pericardial pressure and right atrial pressure: an intraoperative study. *Circulation* 1986; **73**(3): 428–432.
22. Carlsson M, Cain P, Holmqvist C, *et al*. Total heart volume variation throughout the cardiac cycle in humans. *Am J Physiol Heart Circ Physiol* 2004; **287**: H243–H250.
23. Hamilton DR, Dani RS, Semlacher RA, *et al*. Right atrial and right ventricular transmural pressures in dogs and humans: effects of the pericardium. *Circulation* 1994; **90**: 2492–2500.
24. Faehnrich JA, Noone RB, Jr, White WD, *et al*. Effects of positive-pressure ventilation, pericardial effusion, and cardiac tamponade on respiratory variation in transmitral flow velocities. *J Cardiothorac Vasc Anesth* 2003; **17**(1): 45–50.
25. Smiseth OA, Thompson CR, Ling H, *et al*. A potential clinical method for calculating transmural left ventricular filling pressure during positive end-expiratory pressure ventilation: an intraoperative study in humans. *J Am Coll Cardiol* 1996; **27**(1): 155–160.
26. Rendon DB, Rojas Ojeda JL, Crespo Foix LF, *et al*. Mapping the human body for vibrations using an accelerometer. *Conf Proc IEEE Eng Med Biol Soc* 2007; **2007**: 1671–1674.
27. Shechter G, Resar JR, McVeigh ER. Displacement and velocity of the coronary arteries: cardiac and respiratory motion. *IEEE Trans Med Imaging* 2006; **25**(3): 369–375.
28. Pan J, Tompkins WJ. A real-time QRS detection algorithm. *IEEE Trans Biomed Eng* 1985; **BME-32**(3): 230–236.
29. Schneider M, Stevens C. Development and testing of a new magnetic-tracking device for image guidance. In *Proc SPIE Med Imaging 2007: Visualization and Image-Guided Procedures*, 2007.
30. Cuvillon L, Gangloff J, de Mathelin M, Forgione A. Toward robotized beating heart TECABG: assessment of the heart dynamics using high-speed vision. *Springer LNCS* 2005; **3750**: 551–558.

DOI: 10.1002/rcs